THE JOURNAL OF PHYSICAL CHEMISTRY B

Article

Excitation Energy Trapping and Dissipation by Ni-Substituted Bacteriochlorophyll a in Reconstituted LH1 Complexes from Rhodospirillum rubrum

Petar Haralampiev Lambrev, Yuliya Miloslavina, Ivo H.M. van Stokkum, Andreas D. Stahl, Maciej Michalik, Anna Susz, J#drzej Tworzyd#o, Joanna Fiedor, Gabriella Huhn, Marloes Groot, Rienk van Grondelle, Gy#z# Garab, and Leszek Fiedor

J. Phys. Chem. B, **Just Accepted Manuscript** • DOI: 10.1021/jp4020977 • Publication Date (Web): 09 Jul 2013

Excitation Energy Trapping and Dissipation by Ni-Substituted Bacteriochlorophyll *a* in Reconstituted LH1 Complexes from *Rhodospirillum rubrum*

Petar H. Lambrev[1], Yuliya Miloslavina[1], Ivo H. M. van Stokkum[2], Andreas D. Stahl[2], Maciej Michalik[3], Anna Susz[3], Jędrzej Tworzydło[3], Joanna Fiedor[4], Gabriella Huhn[5], Marie-Louise Groot[2], Rienk van Grondelle[2], Győző Garab[1]*, Leszek Fiedor[3]

[1] *Biological Research Centre, Hungarian Academy of Sciences, Temesvári krt. 62, 6726 Szeged, Hungary*

[2] *Institute for Lasers, Life and Biophotonics, Faculty of Sciences, VU University Amsterdam, De Boelelaan 1081, 1081 HV Amsterdam, The Netherlands*

[3] *Faculty of Biochemistry, Biophysics and Biotechnology, Jagiellonian University, ul. Gronostajowa 7, 30-387 Kraków, Poland*

[4] *Department of Medical Physics and Biophysics, Faculty of Physics and Applied Computer Science, AGH University of Science and Technology, Reymonta 19, 30-059 Kraków, Poland*

[5] *Faculty of Science, Eötvös Loránd University, Pázmány Péter Sétány 1/A, 1117 Budapest, Hungary*

* *corresponding author, E-mail garab.gyozo@brc.mta.hu, Tel. +36 30 433 131, Fax +36 30 433 434*

Abstract

Bacteriochlorophyll *a* with Ni^{2+} replacing the central Mg^{2+} ion was used as an ultrafast excitation energy dissipation center in reconstituted bacterial LH1 complexes. B870, a carotenoid-less LH1 complex, and B880, an LH1 complex containing spheroidene, were obtained via reconstitution from the subunits isolated from chromatophores of *Rhodospirillum rubrum*. Ni-substituted bacteriochlorophyll *a* added to the reconstitution mixture partially substituted the native pigment in both forms of LH1. The excited-state dynamics of the reconstituted LH1 complexes were probed by femtosecond pump-probe transient absorption spectroscopy in the visible and near-infrared spectral region. Spheroidene-binding B880 containing no excitation dissipation centers displayed complex dynamics in the time range of 0.1–10 ps, reflecting internal conversion and intersystem crossing in the carotenoid, exciton relaxation in BChl complement, and energy transfer from carotenoid to the latter. In B870 some aggregation-induced excitation energy quenching was present. The binding of Ni-BChl *a* to both B870 and B880 resulted in strong quenching of the excited states with main deexcitation lifetime of ca. 2 ps. The LH1 excited-state lifetime could be modeled with an intrinsic decay time constant in Ni-substituted bacteriochlorophyll *a* of 160 fs. The presence of carotenoid in LH1 did not influence the kinetics of energy trapping by Ni-BChl unless the carotenoid was directly excited, in which case the kinetics was limited by a slower carotenoid S_1 to bacteriochlorophyll energy transfer.

Keywords: carotenoids, light-harvesting, Ni-bacteriochlorophyll *a*, photosynthesis, transient absorption

Introduction

Several fundamental processes occur in the light-harvesting antennas of all photosynthetic systems, including absorption of photons, storage of the excitation energy, then transfer of excitation energy to the reaction centers, and energy losses via radiative or radiationless decays. Understanding the function of the photosynthetic apparatus cannot be complete without a thorough mechanistic treatment of these processes and their effects on the entire system. Light-harvesting antennas, on the one hand, are designed for minimal quantum losses in order to allow for efficient energy transfer. On the other hand, most photosynthetic organisms actively regulate and make use of the thermal dissipation in the antenna for protection against harmful excess radiation[1,2]. In light-harvesting pigment-protein complexes the energy of the electronically excited pigments, chlorophylls or bacteriochlorophylls (BChls), is dissipated via internal conversion and intra- and intermolecular vibrational relaxation[3] involving vibrational modes of the pigment and its protic and lipidic environment. This creates vibrationally hot molecules, which can be intermediates in various secondary reactions affecting the structure and function of the antennas via the so-called hot-molecule[4] or thermo-optic[5] mechanism. In this work we explore the use of purple bacterial LH1 complexes reconstituted with Ni-substituted BChl *a* (Ni-BChl) as a model system for investigating the thermal dissipation processes in photosynthetic antennas. The substitution of the central Mg^{2+} ion in BChl *a* with Ni^{2+} leads to a dramatic shortening of the pigment's excited-state lifetime, from 3 ns to less than 100 fs[6,7] without significantly altering its ground state properties. Because of the rapid excitation redistribution in bacterial antenna complexes (see below), a Ni-BChl molecule bound to the complex can then serve as an ultrafast excitation energy trap[8,9] that focuses the dissipation process in both space and time, thus potentially facilitating unique spectroscopic investigation. Importantly, as shown in our recent study[10], the excitation reaching the Ni-analog of BChl *a* is very promptly and with 100% efficiency

converted into heat and dissipated to the surrounding, due to the peculiar bonding between Ni^{2+} ion in the central pocket of the pigment.

LH1, the core light-harvesting antenna of purple photosynthetic bacteria[11-15], is a membrane-integral pigment-protein complex noncovalently binding BChl *a* or *b* and carotenoids (Crts) and is characterized by a strong near-infrared absorption band (usually 870-890 nm in BChl *a*-containing species, corresponding to BChl Q_y transition). LH1 surrounds the reaction center (RC) and collects light energy either directly or via energy transfer from the peripheral antenna LH2. The basic building module of the LH1 complex is the α,β-heterodimer consisting of two polypeptides, two BChl *a* and a single Crt molecule[16]. B870, the Crt-less form of LH1, can be reversibly dissociated into and reassembled from heterodimeric subunits B820, termed after the position of their main absorption maximum[17,18]. Isolated B820 subunits can bind Crts which strongly promote their association, first to an intermediate iB873 in the presence of sub-stoichiometric amounts of Crt, and then to B880[19,20]. Analysis of 2D crystals of reconstituted LH1 and native LH1-RC complexes from *Rhodospirillum rubrum*[21,22] has revealed 16 heterodimer units containing 32 BChls, arranged in a closed circle with an overall diameter of 116 Å. Several factors are responsible for the absorption shifts from 780 nm, through 820 nm and 870/880 nm, apparently related to the aggregation state of BChl[11,13]. Most notably, it is the strong Coulombic interaction, or excitonic coupling, between the pigment molecules[23] but also the dielectric properties of the environment, H-bonds and other interactions with the apoprotein and charge-transfer states[24,25]. In addition to the altered absorption wavelength, excitonic interactions in the antenna have far-reaching consequences on its light-harvesting function by broadening the absorption band, increasing the dipole strength (superradiance)[26], and providing the physical mechanism for ultrafast excitation energy transfer (EET)[15,27-31], which occurs with a near unity

efficiency in the purple bacterial photosynthetic unit and delivers energy to the RC within tens of ps[32-34].

According to the disordered exciton model[35], the Q_y absorption of LH1 is dominated by a few low-energy exciton states. In each of those states the energy is delocalized over several (or all) BChls. There has been much controversy over the delocalization size (also termed coherence length) in LH1 and LH2. Most authors agree that, due to disorder breaking the ring's symmetry and site degeneracy, the excited state is localized over 3–4 BChls[26,36-40]. However, there are also experimental evidences that the energy is delocalized over the entire BChl ensemble[41]. In isolated LH1 the energy redistribution is complete within about 0.5 ps and the equilibrated excited state has a lifetime of 0.7 ns. The carotenoids binding to LH1 can also serve as light-harvesting pigments by transferring absorbed energy to BChl[15,42,43]. The optically excited S_2 state ($1B_u^+$) is energetically close to the Q_x transition of BChl and the transition dipole moments are nearly parallel, hence the main energy transfer pathway is typically $S_2 \rightarrow Q_x$, which in LH2 has been found to occur on a time scale of 50–250 fs[28,43,44] and about 200 fs in LH1[45]. Despite the rapid EET, the efficiency of this pathway can be low because it competes with the fast internal conversion to the Crt S_1 state. A secondary EET pathway is $S_1 \rightarrow Q_y$, generally much slower since the S_1 state has very low oscillator strength[42,46,47]. The $S_1 \rightarrow Q_y$ rate has been estimated for various carotenoids and LH complexes to lie between $(1.5\ \text{ps})^{-1}$ and $(30\ \text{ps})^{-1}$ [47,48]. The efficiency of this EET pathway is determined by the lifetime of the given Crt's S_1 state – typically several ps. Additional pathways of Crt→BChl EET may involve the dark Crt states lying between S_2 and S_1 – $1B_u^-$, S*, etc.[49] In their model of the transient absorption data of reconstituted LH1, Akahane et al.[45] proposed that $1B_u^- \rightarrow Q_x$ EET is active in LH1 with neurosporene and spheroidene, in addition to the other two EET pathways. In spite of the abundancy of quantum chemical calculations and experimental data, the Crt and Crt–BChl excited-state dynamics remain not fully understood.

In this work we investigated the dynamics of EET and energy trapping by Ni-BChl incorporated in LH1 reconstituted both with and without Crts. As Crts are known to mediate the formation and stabilize the structure of the oligomeric LH1[19,50,51], we have addressed a question of how the presence of Crt in LH1 affects the energy trapping by Ni-BChl.

Experimental Methods

Preparation of carotenoid-less LH1

Rhodospirillum rubrum strain G9 (lacking carotenoids) was grown under aerobic conditions. Chromatophores were first isolated from the bacterial cells collected from the growing chamber. B820 heterodimers were isolated as described previously[19] by a stepwise solubilization of chromatophores with octyl-ß-glucopyranoside (ß-OG, analytical grade, Anatrace, USA). Ni-BChl *a* was prepared by transmetallation method as described[7]. Purified Ni-BChl *a* dissolved in acetone was added in small aliquots so that the absorbance of Ni-BChl in the final solution was 20% of the absorbance of B820. The final acetone concentration was 5%. The sample was further incubated for 4 h at room temperature under slow agitation. The Ni-substituted and non-substituted (control) B820 samples were purified by ion-exchange chromatography on a column of fast-flow DEAE Sepharose (Sigma, USA). After complete absorption of the sample, the column was washed with 20 mM TRIS·HCl buffer (TB) containing 1% ß-OG and increasing amounts of NaCl. The purified B820 complexes were used for the reconstitution of LH1 (B870). Reconstitution was performed by centrifugation in a concentrating filter device with 10 kDa cutoff (Amicon Ultra, Millipore, USA). Because the micelle molecular weight of ß-OG is 8 kDa, during the centrifugation the detergent concentration in the retentate gradually decreases. B870 is formed near the CMC, washed repeatedly with TB (pH 8.0) and finally resuspended in buffer with 0.4% ß-OG to obtain absorbance at 870 nm of ~10 / mm.

Prior to spectroscopic measurements, the ß-OG concentration was increased to 0.7% to minimize large-scale aggregation. The sample was thoroughly mixed and sonicated for one minute to achieve homogeneity.

Reconstitution of LH1 with spheroidene

Isolation of native LH1, extraction of carotenoids, and reconstitution of LH1 with spheroidene was done according to the procedures described previously[51]. To obtain Sph-LH1 substituted with Ni-BChl, before adding Sph to the reconstitution mixture, a portion of 19.8 μg Ni-BChl dissolved in 200 μl of acetone was added to 50 ml of LDAO-dissociated Crt-less chromatophores (containing 72 μg of BChl *a*) and the solution was incubated for one hour at ambient temperature. The reconstitution mixture was loaded on a small DEAE-cellulose (DE52, Whatman, UK) column and the fraction of purified LH1 was eluted with 20 mM TB (pH 7.8) containing 0.2 M NaCl and 0.45% LDAO (analytical grade, Fluka, Switzerland), and then concentrated (5-10-fold) using centrifugal concentrating devices (Amicon Ultra, Millipore, USA). 30 kDa cut-off filters were necessary in this case for empty detergent micelles to pass through.

Pigment stoichiometry

For the analysis of pigment composition, aliquots of the B870 and B880 complexes were loaded onto a small column of DEAE-sepharose FastFlow (B870) or DEAE-cellulose DE52 (B880) equilibrated with the respective buffers. The column was rinsed with distilled water to remove the detergent and the pigments were extracted with acetone and dried under vacuum. Prior to HPLC analysis, the extracts were dissolved in a mixture of 99.85% toluene/0.1% 2-propanol/0.05% methanol. Pigment composition of the extracts was analyzed as described previously[9], using a Prostar HPLC system (Varian, USA), equipped with a 5 μm Si-60 LiChrospher column (250×4.6 mm, Merck, Germany) and a TIDAS diode array detector (J&M Analytik, Germany). Pigment

identification was based on absorption spectra and retention times of pure BChl *a*, Ni-BChl and Sph. The detailed analytical procedure will be described elsewhere.

Absorption and fluorescence spectroscopy

Absorption spectra were measured in a 1 mm quartz cell using Cary 50 spectrophotometer (Varian). Steady-state fluorescence emission spectra were recorded at 17°C in 1 cm cells, on a Fluoromax-P spectrofluorometer (Horiba, Japan), equipped with a 0.22 m double monochromator and a cooled infrared-extended PMT detector.

Femtosecond transient absorption spectroscopy

Room-temperature TA experiments in the visible and near-infrared (NIR) spectral ranges were performed with a setup described in more detail in Pawlowicz et al.[52]. Briefly, the output of a Ti:Sapphire regenerative-amplified laser system (Hurricane, SpectraPhysics, USA), operating at 1 kHz and producing 85 fs, 800 nm pulses, was divided into two beams. One beam was sent to a homebuilt noncollinear optical parametric amplifier (NOPA) system to generate the excitation pulse at the desired center wavelengths of 509, 590-600 and 860 nm. A narrow bandwidth and high conversion efficiency in the NOPA were obtained by placing an appropriate interference filter in the path of the white-light seed of the NOPA. The pump beam was polarized at the magic angle orientation (54.7°) with respect to the probe beam with a Berek polarizer. The excitation pulse from the NOPA was focused at the sample with a spot diameter of ~120 μm and spatially overlapped with the probe beam. A phase-locked chopper operating at 500 Hz ensured that only excited every other shot and the changed in transmission and hence optical density could be measured. The time delay between pump and probe beams was controlled by sending the pump beam over a moveable delay line.

The probe beam was focused on a 2-mm sapphire plate to generate white light continuum. After passing through the sample, the probe beam was dispersed onto a 2068-channel CCD detector. The sample was placed in a cell consisting of two CaF_2 windows separated by 50 µm Teflon spacer. The absorbance was measured to be 0.45–0.7 µm at the Q_y region. The sample was moving during the measurement in a Lissajous pattern to ensure a fresh spot for every excitation pulse.

The time-resolved data were subjected to global and target analyses[53] using the Glotaran software[54].

Atomic Force Microscopy

Muscovite mica sheets (Grade V-5) purchased from SPI Supplies (USA) were chosen as a support for the samples. Few µL of Crt-less LH1 solution (in TB containing 0.4% ß-OG) was pipetted directly onto the surface of freshly cleaved mica. Following deposition, the mica sheet was placed in enclosed Petri dishes for several hours in order to evaporate the excess of water. Analysis of samples was done using a Solver PRO scanning probe microscope (NT-MDT Ltd., Russian Federation). The surface scanning was performed in a semi-contact (tapping) mode to avoid altering the sample in subtle ways. The images presented were processed by applying a low-pass filter.

Results

Reconstitution of LH1

In this work we applied two different methods for reconstitution of oligomeric LH1 complexes from *Rsp. rubrum*. In the first, Crt-less LH1 (B870) was obtained from the Crt-less mutant G9 and reconstituted by decreasing the concentration of detergent (β-OG) below its critical micellar

concentration. An inevitable consequence is that the reconstituted complexes are aggregated. In the second method, oligomerization was induced by adding Crt (spheroidene) in the presence of detergent (LDAO). With both LH1 types BChl *a* was partially substituted with Ni-BChl *a* and additionally control LH1 samples were prepared without adding Ni-BChl. The absorption spectra of representative samples are shown in Figure 1. The spectra of Crt-less LH1 have three BChl bands – at 375 nm (B-band), 590 nm (Q_x) and 870 nm (Q_y). In Sph-LH1 the Q_y maximum was found at 880 nm[51], as for native LH1 from *Rsp. rubrum*. In addition, the three vibronic bands (443, 470, 503 nm) of the $S_0 \rightarrow S_2$ transition of Sph are visible in the Sph-LH1 spectra and the 366 nm maximum indicates some small contamination of Crt aggregates. The samples containing Ni-BChl had generally similar spectra, the differences reflecting mainly batch-to-batch variability.

In the spectra shown in Fig. 1, additional low intensity bands can be seen in the Q_x region. One, located near 540 nm (Fig. 1A), is contributed by the Ni-substituted BChl *a*. The other band, at 550 nm, seen in the Sph-LH1 spectra (Fig. 1B) is most likely due to the vibrational side band of the Q_x band of BChl *a* in LH1[55].

The Crt-containing Sph-LH1 complexes were stable at concentrations of LDAO above the CMC and hence could be studied in a detergent-solubilized, non-aggregated state. Crt-less LH1 dissociates at the CMC and could be only obtained in a partially aggregated state (below the CMC). The structural integrity of the oligomeric B870 (Crt-less LH1) complexes in this case was checked by atomic-force microscopy (Fig. 2). The LH1 rings are clearly visible on the images. The rings had average diameters of 20 nm and 25 nm (see Supporting Information, Fig. S1). No differences could be detected between control LH1 (not containing Ni-BChl) and Ni-LH1 (containing Ni-BChl).

The successful integration of Ni-BChl in the LH1 complexes was confirmed by monitoring the fluorescence yield of control and Ni-LH1. The fluorescence was excited at 590 nm and spectra were recorded from samples diluted to the same optical density. The relative fluorescence yield was estimated by integrating the main fluorescence band. The relative yields of emission from Ni-LH1 were lower 17- to 33-fold (the signal intensity was 6–3% of the control LH1's fluorescence) in both types of LH1 – Crt-less and Sph-LH1 (data not shown).

To determine the pigment stoichiometry in the reconstituted complexes the HPLC method was employed. Based on peak intensities at 467 nm and 790 nm in the chromatograms of the B870 and B880 extracts, the amounts of the incorporated Ni-BChl were calculated and they were 19.5% and 14.7% of the total BChl content, respectively. The ratio of total BChl to Sph was 2:0.89 in the control B880 and 2:0.91 in the Ni-BChl substituted complex.

Pump-probe transient absorption spectroscopy

The excited-state dynamics of LH1 was studied by femtosecond pump-probe TA spectroscopy in the visible and NIR region. Considering the steady-state absorption spectra (Fig. 1), pump wavelengths were chosen for selective excitation of either BChl or Sph. For B870 the pump wavelength was set at 590-600 nm, corresponding to the BChl Q_x transition. The measurements on Sph-LH1 were done using three pump wavelengths, 590 nm (BChl Q_x), 860 nm (BChl Q_y), and 509 nm (Sph S_2, 0-0 transition). The absorption difference was probed in the NIR region for all wavelengths. In addition, with pump wavelength of 509 nm, the absorption was probed in the visible region, in order to reveal the dynamics of Crt excited states.

The NIR transient absorption spectra were characterized by a negative band at 880–890 nm due to BChl ground-state bleaching and stimulated emission (SE) and a positive band at 840–860 nm, corresponding to BChl excited-state absorption (ESA). The transient kinetics at the negative

maximum after excitation in the BChl Q_x region are shown in Fig. 3A – Crt-less LH1 and Sph-LH1, and in Fig. 3B for Crt-less Ni-LH1 and Sph-Ni-LH1. In control samples the TA signal rose to its maximum between 1 and 10 ps and then decayed due to the recovery of the ground state. There was no detectable loss of the bleaching signal up to ca. 40 ps in Sph-LH1. The decay phase was substantially faster in Crt-less LH1, probably due to the complex aggregation at low concentrations of the detergent.

The rapid quenching of excitations by Ni-BChl is apparent from the kinetic traces shown in Fig. 3B. In LH1s reconstituted with Ni-BChl, the pump-probe signal decayed to 30–40% of its maximum within 10 ps, which is in a strong contrast to control LH1 whereof no significant decay was observed in this time range. Despite the much faster decay, the multiexponential decay of the transient absorption was clearly resolved in our measurement. Moreover, we could still follow the build-up of the absorption signal in the first picosecond after excitation, before the onset of excited-state deactivation (quenching), which gives us confidence that even the fastest quenching components could be resolved in this measurement. Comparison of the kinetic traces for Crt-less and Sph-LH1, when excited directly to BChl, reveals only small differences, viz. slightly faster decay in the Crt-less sample that was however within the differences between preparations.

Figure 4 compares kinetic traces probed at the wavelength of the maximal negative differential absorption of Sph-LH1 for pump wavelengths of 509 nm, 590 nm, and 860 nm, corresponding to the Sph S_0–S_2, BChl Q_x, and BChl Q_y electronic transitions, respectively. Note that the orange curves are identical in Figs. 3 and 4. Not surprisingly, the kinetics in the NIR (BChl Q_y) region were faster when the Q_y transition was invoked directly by the pump pulse and slower when the pump wavelength was tuned to the higher-energy Q_x transition. In the latter case the rise components of the NIR TA in the first ps clearly correspond to $Q_x \rightarrow Q_y$ internal conversion. Rise components due to Crt→BChl EET could be anticipated in the same time region upon excitation

of the Crt. Interestingly, the TA at 509 nm excitation showed a well-discerned multi-phasic slow rise of the BChl bleaching, observable up to ca. 20 ps. The Ni-BChl-containing LH1 also showed distinct excitation wavelength dependence of the excited-state kinetics. The fastest decay of the excited state was observed upon the Q_y excitation. Somewhat slower was the decay upon the Q_x excitation and it was markedly slower upon excitation of Sph. For instance, at time delay of 5 ps, the amplitude of the bleaching signal was reduced by 60% after BChl Q_y excitation while only by 20% after Sph excitation.

Global analysis of the TA data

The time- and wavelength-dependent absorbance data were subjected to a global iterative fitting routine applying a sequential kinetic model with 4–5 components of increasing lifetimes. The fitting was done by variable projection, i.e. the lifetimes were fitted as nonlinear parameters by iterative matrix decomposition and the lifetime/evolution-associated absorption difference spectra (EADS) were treated as linear parameters. Additionally, the model accounted for dispersion (chirping) and temporal convolution with the instrument response function. The resulting spectra and corresponding lifetimes are presented in Fig. 5 (590 nm excitation) and Fig. 6 (509 nm excitation). The initial spectra (in black) represent the directly excited state, i.e. Q_x in Fig. 5 and Sph S_2 in Fig. 6. As the fastest lifetimes are comparable to the pulse width, the shape of the respective spectra is somewhat affected by pump–probe overlap and their amplitude reflects the relatively large error in the fitted lifetime. The spectra in the NIR are blue-shifted, lack SE on the long-wavelength side but show positive ESA instead, in accordance with previous pump-probe results on LH1[56,57]. The following NIR spectra, associated with longer lifetimes, represent excitonic states in the Q_y band, populated after $Q_x \rightarrow Q_y$ internal conversion. The following equilibration and relaxation in the exciton manifold results in spectral changes, visible in control LH1 (Fig. 5A and 5B), i.e. the amplitude increases (compare the 1 ps and 20 ps EADS in Fig. 5A

and the 0.27 ps and the 10 ps EADS in Fig. 5B), the negative maximum shifts to longer wavelengths, and the appearance of SE broadens the spectra on the long-wavelength side[56]. In Sph-LH1 the lifetime associated with exciton relaxation was 270 fs, very close to previously reported values. An additional, a much slower (10 ps) component was detected, which probably reflects vibrational relaxation. Note that the spectral evolution in Sph-LH1 (Fig. 5B) proceeds without any loss of overall amplitude, which would signify excitation decay. There's only one decay component with 0.75 ns lifetime, which is in good agreement with the excited-state decay in native LH1 from *Rhodobacter sphaeroides*[58] and native and reconstituted B875 from *Rubrivivax gelatinosus*[59]. In contrast to Sph-LH1, the TA of Crt-less LH1 did not decay monoexponentially but two additional lifetimes were present, of 20 and 100 ps. The result is in accordance with the 0.39 ns fluorescence lifetime of *Rsp. rubrum* B873, as determined by Chang et al.[60], and which, as mentioned above, can probably be explained by aggregation-induced excited state quenching.

On sub-ps time scale, Ni-LH1 showed similar spectral evolution reflecting internal conversion as the control LH1 (Fig. 5C, D). The follow-up spectra also have very similar shape as the respective control LH1 spectra. No sub-ps decay components could be resolved but only exciton equilibration components, as with the control samples. These were omitted in the presented spectra since they did not significantly improve the fit. The excitation trapping by Ni-BChl is manifested in the picosecond decay lifetimes. The major decay lifetimes were 3.2 and 2.5 ps for Crt-less Ni-LH1 and Sph-Ni-LH1, respectively. The amplitudes of the following EADS (40 ps in 5C and 14 ps in Fig. 5D) were lower by 60–70%, indicating that the 2–3 ps decay components were responsible for quenching of 60–70% of the excitations. Still, significant proportion of the excited states decayed on a much slower time scale, mainly through the 40 ps component (Crt-less Ni-LH1) and the 100 ps component (Sph-Ni-LH1). At closer inspection the spectra of these slower components appeared blue-shifted by ~3 nm, compared to the spectra of the main quenching component. This

may be a hint that they originate from a structurally different population of complexes in the sample, or, alternatively, from different excited states. Perhaps this heterogeneity was present also in the control samples but was not resolved kinetically because of the uniform decay lifetime.

Upon Sph excitation (509 nm), the initial NIR spectra (Fig. 6A, B) were significantly blue-shifted and exhibited positive ESA around 920 nm. This ESA can be attributed to the short-lived S_2 and hot S_1 states of Sph as well as BChl Q_x states populated via EET from Sph. The subsequent evolution in the control Sph-LH1 is spectrally very similar as with 590 nm excitation, showing a gradual red shift, broadening and increase in overall amplitude due to the population of emitting low-energy excitonic states in the Q_y region. The associated lifetimes are however significantly longer, which probably reflects the slower Sph→Q_y EET pathways. The decay of BChl excited states was again monoexponential with a 0.67 ns lifetime but the best fit was achieved by adding a long-lived (>>1 ns) ESA component that can be attributed to the Crt.

As the above-described transients show, the decay kinetics of Ni-LH1 was affected by excitation wavelength. The lifetime of the fastest quenching component was 4.6 ps with 509 nm excitation, as compared to 2.5 ps with 590 nm. Moreover, a smaller proportion (36%) of the ground state bleaching was recovered by this kinetic component. The slower lifetimes did not differ between 509 and 590 nm excitation and the associated spectra were again blue-shifted by 3 nm.

The transient absorption in the visible range, revealing dynamics of the Crt excited states, was measured and analyzed independently with a 4-component sequential model (Fig. 6A, C). The initial spectra, assigned to Sph S_2 state ($1B_u^+$) clearly show bleaching of the S_0→S_2 transition band. The S_2 state decays with a 120 fs lifetime. The following spectrum, associated with a 2 ps lifetime, has ESA maxima at 525 nm and 550 nm, corresponding to triplet state and S_1 ($2A_g^-$) state, respectively. The 17-19 ps component has higher contribution of triplet state and also a

shoulder at ~540 nm, which could be attributed to either the S_1 or S* state. The longer-lived component spectra are unambiguously assigned to ^{3}Sph. The Crt lifetimes match closely the kinetics in the BChl region. This indicates that EET from Crt to BChl occurs via multiple pathways with time constants from ~100 fs to ~20 ps. Evidently the Crt dynamics was not affected by the presence of Ni-BChl in Ni-LH1.

Global target analysis

The above presented analysis of the data provides an estimate of the lifetimes and the general dynamics of the system under different excitation wavelengths but it obviously does not accurately depict the multiple pathways of energy transfer between pigments and excited states and hence cannot give a detailed account on the specific EET rate constants and spectra. We have therefore performed target analysis of the pump-probe data of Sph-LH1 and Sph-Ni-LH1 with a branched model. The kinetic scheme used for fitting the Sph-Ni-LH1 data is shown in Fig. 7. A very similar scheme plus exciton relaxation components was used for fitting the control Sph-LH1 data (Supporting information, Fig. S2). The model was fitted to the pump-probe data obtained with the three pump wavelengths simultaneously with the same set of rate constants, only varying the initially populated excited states. The species-associated absorption difference spectra (SADS) were estimated independently for each excitation and probe wavelength range and are plotted in Fig. 8 for Sph-Ni-LH1. The respective control LH1 SADS are shown in Fig. S3 (Supporting Information). The quality of the fits is demonstrated in Figs. S4 and S5.

In the kinetic scheme we distinguish four Crt states, S_2, S_1, S*, and T_1. There are two pathways for Crt→Bchl EET: from S_2 to Q_x and from S_1 to Q_y. Four BChl states were needed to fit the kinetics of control LH1. One of them describing the directly excited BChl* (Q_x or Q_y^0) and three subsequent states to describe the exciton relaxation (cf. Fig. S2) and spectral evolution. The exciton relaxation was not explicitly modeled for the Ni-LH1 data. The quenching by the Ni-BChl

centers is quantified by the amplitudes of the BChl SADS and by the rates describing their spectral evolution. In this way the data with the Crt, BChl Q_x and BChl Q_y excitation were simultaneously fitted. The estimated rate constants are indicated in Fig. 7. The control sample exhibited a subtle spectral evolution (red-shift), reflected in the SADS (Fig. S3) and also evident from the selected traces and fits in Fig. S4. The final SADS decays in 0.7 ns. In contrast, the Q_y compartment decayed with a 2 ps lifetime in the Ni-LH1 sample but two additional time scales were required to describe the quenching. This apparent heterogeneity is modelled by two compartments (populated as Q_y), with lifetimes of 12 and 108 ps. The fraction of these more slowly quenched complexes varied between 21–31% for the different datasets (see Table 1). The dominant fraction quenched within 2 ps varied between 42 and 55%. The SADS of the more slowly quenched complexes, and especially the longest-lived one (108 ps), were blue-shifted, compared to the main Q_y SADS.

Discussion

Reconstitution of LH1

In this work we employed two reconstitution techniques to incorporate Ni-BChl into LH1 from *Rsp. rubrum*. In the first, Crt-less LH1 (B870)[19] are assembled mostly due to hydrophobic interactions between the N-terminal extensions of the α and β polypeptides at the membrane interface[61,62]. In the second method, Crts specifically interact with the subunits and promote complex formation under conditions where Crt-less complexes dissociate[19,20,51]. The B870 complexes are structurally similar to the native, Crt-binding LH1 antenna, as can be seen from AFM images (Fig. 2) but there are also some differences, e.g. the NIR absorption maximum is blue-shifted by 10 nm relative to its 880 nm position characteristic for the strain[19,51,63]. The shift of the excitonic transition's wavelength could be accompanied by altered energy transfer and

hence energy trapping dynamics. A consequence of the Crt-less LH1 reconstitution method is a higher level of aggregation. We strived to minimize the size and heterogeneity of the aggregates by carefully adjusting the concentration of the detergent and applying mechanical and ultrasonic homogenization before measurements. However, even small aggregates may have a profound effect on the energy transfer dynamics because of energy migration between B870s. The larger effective domain size raises the likelihood of nonlinear (two-photon) reactions such as exciton-exciton annihilation[64]. This can be one possible explanation for the fast excited state decay lifetimes (20–100 ps) in our Crt-less LH1 preparations. Since exciton-exciton annihilation strongly depends on the excitation rate, we performed test measurements reducing the excitation power by up to one order of magnitude, but did not observe any appreciable differences in the kinetic traces, other than the reduction of signal-to-noise ratio (data not shown). It is possible that the excited state lifetime is shortened by dissipative states formed by interactions between the aggregated complexes. Interestingly, shorter excited-state lifetimes were found in carotenoid-less LH2 compared to native complexes from the purple bacterium *Allochromatium minutissimum*[65]. The authors proposed that in the absence of carotenoids BChl triplets could accumulate and quench the excited states via singlet-triple annihilation. Such a mechanism can't be completely ruled out but again should be dependent on the excitation rate, which we could not confirm. Lastly, small amount of excited state quenchers could be present such as oxidized BChls, whose effect would be larger in the aggregated Crt-less LH1 where energy can migrate between complexes.[66]

Excited state dynamics of control LH1

The LH1 complexes reconstituted with Sph were stable in detergent solution (0.45% LDAO), showing neither scattering nor aggregation. Furthermore, the NIR absorption maximum matched that of the native antenna (880 nm) and so did the excited-state lifetime (0.7 ns). The absence of

any faster decay components in the transient absorption confirmed that no exciton-exciton annihilation took place under the measurement conditions. Thus, we have obtained a detailed, high-resolution spectroscopic picture of the ultrafast dynamics in LH1, devoid of nonlinear processes and aggregation-related artifacts.

The TA data reveal the exciton relaxation dynamics occurring on a sub-ps time scale. The position of the negative band in the time-resolved spectra shifted to longer wavelengths, its overall amplitude increased and the band was asymmetrically enhanced on the long-wavelength side due to SE following the population of lower-energy emitting excitonic states by internal conversion from the initially populated states. A similar dynamic red shift was found by Visser et al.[56] in the TA kinetics of LH1 from *Rsp. rubrum* after excitation in the BChl Q_x region. As in our results, it occured with a ~300 fs time constant and was attributed to relaxation in the exciton manifold. Monshouwer et al.[57] observed a similar spectral change in LH1 from *Rps. viridis*. In addition to the earlier findings, owing to the lack of annihilation, we could detect a further 10-ps spectral equilibration component in Sph-LH1 (Fig. 5B), that could be related to vibrational relaxation and slower reorganization of the environment[67,68]. Even slower (20 ps) lifetimes were found in the spectral evolution of BChl upon excitation of Sph. An obvious explanation for these lifetimes is that they stem from a slow Sph→BChl EET.

Analysis of the transient absorption in the NIR as well as the visible range could provide clues about the dynamics of the Crt excited states and EET pathways, apparently a complex and controversial topic of research[49]. Even though there is a small overlap between the optical transitions of Crts and BChl, several pathways of Crt→BChl EET are possible. The energy of the S_2 state is in the range of the BChl Q_x transition and $S_2 \rightarrow Q_x$ EET occurs with a time constant of 60–240 fs[28,42,44]. Our data revealed fast lifetimes (120-200 fs) in the NIR and in the visible range that could be unequivocally assigned to S_2 decay and concomitant excitation of BChl via the Q_x

state. Fitting the TA data in the visible range with a simple unbranched model revealed lifetimes of ~2 and 20 ps that matched the NIR dynamics (1.3 and 25 ps). An inspection of the associated spectra hinted towards the decay of Sph S_1 state in the visible wavelength range and the population of emitting BChl excitonic states in the Q_y range. The lifetimes and the shape of the visible-range spectra are very similar to those obtained by Gradinaru et al. from *Rsp. rubrum* chromatophores[69] except that the Crt absorption maxima are at different wavelengths because the native LH1 contains spirilloxanthin instead of Sph. The authors found that the S_1 lifetime of spirilloxanthin (1.4 ps) was the same in solution and in the LH1 and concluded that this state was not involved in EET. Considering that the S_1 lifetime of Sph in solution is 9 ps, the 2 ps lifetime in our experiments further corroborates the existence of EET from S_1. The unbranched model fitting also resolved a long-lived (>>1 ns) component in the visible range, which, based on the EADS, clearly belonged to the triplet state of Sph.

Based on the above considerations, target analysis was performed with a branched kinetic model (Fig. 7) fitting the rate constants of internal conversion and intersystem crossing among Sph and BChl states as well as of $S_2 \rightarrow Q_x$ and $S_1 \rightarrow Q_y$ EET. The latter two are $(230\ \text{fs})^{-1}$ and $(3.7\ \text{ps})^{-1}$, respectively. Small differences notwithstanding, the control sample's modeling results conform to literature data on the Crt dynamics in LH2 and LH1. The efficient singlet-to-triplet conversion found by Gradinaru et al.[69] and Papagiannakis et al.[70,71] is confirmed in our data. These papers also reported a state with SADS maximum at 525 nm, like the triplet state, but with a broader long-wavelength shoulder. It decays with a time constant of 70 ps to the triplet and to the ground state. Our data are consistent with these findings, with respect to the SADS and lifetime of this state, which was ascribed to S*. Koyama's group has published a TA investigation of LH1 reconstituted with different Crts[45]. They resolved an intermediate state between S_2 and $S_1 - 1B_u^-$, which is precursor to the T_1 state. The evolution kinetics and the SADS differ from the S* state in

the present model, hence probably these are different intermediates. The remaining SADS are very similar and so are the fitted rate constants of Sph internal conversion and Sph→BChl EET.

Dissipation of excitations by Ni-BChl

The steady-state fluorescence and the TA results of LH1 complexes containing Ni-BChl showed the expected strong quenching, in samples with and without Crts. Interestingly, the kinetics were heterogeneous with lifetimes ranging from 2 ps to 100 ps. The main dissipation channel, with about 50% fractional amplitude, appeared to be $(2\ ps)^{-1}$. Faster excited-state decay components were not resolved in the TA data, even upon direct excitation in the Q_y exciton band. These results are in contrast to the previously reported TA study by Fiedor et al.[8], in which *Rb. sphaeroides* B870 complexes containing 20% or more Ni-BChl showed a 60 fs deactivation lifetime. This difference can be partly explained by a smaller ring in this reconstituted LH1, estimated to be close to 20 BChl a molecules[8,9]. Sub-ps kinetic components were present in the data but they were associated with internal conversion among excited states. Therefore it can be concluded that the excited states directly populated by the pump pulse, i.e. Q_x and higher-energy excitonic states, are not trapped by Ni-BChl – which is not surprising, since the excitations must first migrate to the quencher molecules.

To understand the origin of the 2 ps decay lifetime one must consider three factors determining the deactivation kinetics – the intrinsic deactivation rate constant of the Ni-BChl centers k_q, the number of Ni-BChl molecules in the complex N_q, and the mean effective rate constant of energy transfer (hopping) between BChls, k_h. In reality all four parameters N, N_q, k_q, k_h should be (broad) distributions rather than single values, considering the static and dynamic disorder in the system[72]. As a simple example, let all complexes consist of 32 total BChls and one Ni-BChl with k_q = 16 ps^{-1}. Let us further assume instantaneous energy equilibration ($k_h = \infty$), i.e., the excitations are delocalized over the whole complex. The excited-state lifetime of the complex will be

$$\tau = 1 / (k_q * N_q / N) = 2 \text{ ps.}$$

The relative content of Ni-BChl in the samples was 12–15%, equivalent to about four Ni-BChls per complex, on average. Taking into account the Poisson statistical distribution, the estimated average lifetime is 0.66 ps. Thus, a model assuming fully delocalized excitations and 60 fs dissipation time constant of Ni-BChl cannot explain the experimental results. An intrinsic dissipation rate constant of $(200 \text{ fs})^{-1}$ results in the experimentally observed 2 ps lifetime. This result seems reasonable considering that Musewald et al.[6] performed TA measurements on Ni-BChl in toluene and pyridine and found that the Q_y state mainly decays with lifetime of 450 and 200 fs, respectively. Next, we take into account that the delocalization length may not cover the whole ring, as has been proposed by several groups. We calculated the effective lifetime by treating the excitations as localized[73] and migrating with an effective rate constant of 100 fs[74]. Simulation of the kinetics for 15% average Ni-BChl content resulted in a 2 ps lifetime if the intrinsic deactivation lifetime of Ni-BChl was fixed to 160 fs.

It must be noted that in the above simulations, due to the statistical distribution of N_q, there is also a distribution of decay lifetimes, which may be a reason for the lifetime heterogeneity observed in the TA data. It could be then speculated that the ~10-ps lifetime originates from complexes with only one Ni-BChl and 2 ps is the mean lifetime of complexes with two or more Ni-BChls. The longer, 100 ps, decay lifetimes, most probably reflect partially dissociated complexes, which contain smaller number of subunits and are thus statistically less likely to contain Ni-BChl. The blue-shifted spectra of these components corroborate this notion. As the measurements were performed at high protein concentration, it is likely that EET between complexes takes place and excitations in complexes without Ni-BChl can be quenched by EET to those containing Ni-BChl. Natural disorder could also be the reason for slower migration and relaxation rates[72].

It is notable that the excitation trapping by Ni-BChl was not affected by the presence or absence of Sph in the complexes. It can be thus inferred that also the Crts do not influence the dynamics of EET between BChls in LH1. Only direct excitation of Sph had an effect on the dissipation kinetics, since the kinetics was partially rate-limited by the slower $S_1 \rightarrow Q_x$ EET.

Conclusions

The ultrafast spectroscopy of LH1 complexes reconstituted with Sph are generally in good agreement with literature data regarding native LH1 and LH2 complexes[69-71] as well as of reconstituted Sph-LH1[45]. We found that Crt-less LH1 had shorter excited-state lifetime, probably caused by the lack of detergent and consequent aggregation of the B870 complexes or due to quenching by BChl triplets accumulated in the absence of Crt[65]. The bound Crt did not appear to have a direct effect on the EET among BChls.

The presence of Ni-BChl molecules in LH1 complexes can effectively dissipate the absorbed light energy within a few picoseconds. Only the lowest-energy BChl excited-states can be deactivated by Ni-BChl. The dissipation kinetics is evidently limited by excited state energy equilibration within the complex. Although the dissipation rate is not as fast as previously determined[8], yet it is accelerated by more than two orders of magnitude in comparison to the native antenna, which makes this system a good model for the thermal energy dissipation in pigment-protein complexes. These results are the basis for future investigation of the heat dissipation in pigment-protein complexes reconstituted with the Ni-analogs of (bacterio)chlorophylls by ultrafast vibrational spectroscopy.

Acknowledgement

The project was supported by grants from LaserLab Europe (project LCVU-1606 to PL and YM), the Hungarian Scientific Research Fund (OTKA-PD 104530 to PL, TÁMOP-4.2.2.A-11/1/KONV-2012-0060 to GG), the Hungarian National Innovation Office and A*STAR Singapore (NIH-A*STAR TET_10-1-2011-0279 to GG), the European Commission (EC-MC ITN 238017 HARVEST to GG), the European Research Council (Advanced Grant Proposal 267333 PHOTPROT to RvG), and the Foundation for Polish Science (TEAM/2010-5/3 to LF).

Supporting information available: Figure S1: Distribution of ring diameters estimated from AFM images. Figure S2: Target analysis scheme used for fitting the TA data of control Sph-LH1. Figure S3 and S4: Measured and fitted kinetic TA traces.

REFERENCES

(1) Niyogi, K. K. Safety Valves for Photosynthesis. *Curr.Opin.Plant Biol.* **2000**, *3*, 455-460.
(2) Li, Z.; Wakao, S.; Fischer, B. B.; Niyogi, K. K. Sensing and Responding to Excess Light. *Annu.Rev.Plant Biol.* **2009**, *60*, 239-260.
(3) Bixon, M.; Jortner, J. Intramolecular Radiationless Transitions. *J.Chem.Phys.* **1968**, *48*, 715-726.
(4) Nakashima, N.; Yoshihara, K. Role of Hot Molecules Formed by Internal Conversion in UV Single-Photon and Multiphoton Chemistry. *J.Phys.Chem.* **1989**, *93*, 7763-7771.
(5) Cseh, Z.; Rajagopal, S.; Tsonev, T.; Busheva, M.; Papp, E.; Garab, G. Thermooptic Effect in Chloroplast Thylakoid Membranes. Thermal and Light Stability of Pigment Arrays with Different Levels of Structural Complexity. *Biochemistry* **2000**, *39*, 15250-15257.
(6) Musewald, C.; Hartwich, G.; Lossau, H.; Gilch, P.; Pöllinger-Dammer, F.; Scheer, H.; Michel-Beyerle, M. E. Ultrafast Photophysics and Photochemistry of [Ni]-Bacteriochlorophyll *A*. *J.Phys.Chem.B* **1999**, *103*, 7055-7060.
(7) Hartwich, G.; Fiedor, L.; Simonin, I.; Cmiel, E.; Schäfer, W.; Noy, D.; Scherz, A.; Scheer, H. Metal-Substituted Bacteriochlorophylls. 1. Preparation and Influence of Metal and Coordination on Spectra. *J.Am.Chem.Soc.* **1998**, *120*, 3675-3683.
(8) Fiedor, L.; Scheer, H.; Hunter, C. N.; Tschirschwitz, F.; Voigt, B.; Ehlert, J.; Nibbering, E.; Leupold, D.; Elsaesser, T. Introduction of a 60 Fs Deactivation Channel in the Photosynthetic Antenna LH1 by Ni-Bacteriopheophytin A. *Chem.Phys.Lett.* **2000**, *319*, 145-152.
(9) Fiedor, L.; Leupold, D.; Teuchner, K.; Voigt, B.; Hunter, C. N.; Scherz, A.; Scheer, H. Excitation Trap Approach to Analyze Size and Pigment-Pigment Coupling: Reconstitution of LH1 Antenna of *Rhodobacter sphaeroides* with Ni-Substituted Bacteriochlorophyll. *Biochemistry* **2001**, *40*, 3737-3747.

(10) Pilch, M.; Dudkowiak, A.; Jurzyk, B.; Lukasiewicz, J.; Susz, A.; Stochel, G.; Fiedor, L. Molecular Symmetry Determines the Mechanism of a Very Efficient Ultrafast Excitation-to-Heat Conversion in Ni-Substituted Chlorophylls. *Biochim.Biophys.Acta* **2013**, *1827*, 30-37.
(11) Robert, B.; Cogdell, R. J.; van Grondelle, R. The Light-Harvesting System of Purple Bacteria. In *Light-Harvesting Antennas in Photosynthesis*; Green, B. R., Parson, W. W., Eds.; Kluwer Academic Publishers: Dordrecht, 2003; pp 169-194.
(12) Law, C. J.; Roszak, A. W.; Southall, J.; Gardiner, A. T.; Isaacs, N. W.; Cogdell, R. J. The Structure and Function of Bacterial Light-Harvesting Complexes (Review). *Mol.Membr.Biol.* **2004**, *21*, 183-191.
(13) Cogdell, R. J.; Gall, A.; Köhler, J. The Architecture and Function of the Light-Harvesting Apparatus of Purple Bacteria: From Single Molecules to *in vivo* Membranes. *Quart.Rev.Biophys.* **2006**, *39*, 227-324.
(14) Law, C. J.; Cogdell, R. J. The Light Harvesting System of Purple Anoxygenic Photsynthetic Bacteria. In *Primary Processes of Photosynthesis: Basic Principles and Apparatus*; Renger, G., Ed.; The Royal Society of Chemistry: Cambridge, 2008; pp 205-259.
(15) Hu, X. C.; Ritz, T.; Damjanovic, A.; Autenrieth, F.; Schulten, K. Photosynthetic Apparatus of Purple Bacteria. *Quart.Rev.Biophys.* **2002**, *35*, 1-62.
(16) Cogdell, R. J.; Lindsay, J. G.; Valentine, J.; Durant, I. A Further Characterisation of the B890 Light-Harvesting Pigment- Protein Complex from Rhodospirillum Rubrum Strain S1. *FEBS Lett.* **1982**, *150*, 151-154.
(17) Miller, J. F.; Hinchigeri, S. B.; Parkes-Loach, P. S.; Callahan, P. M.; Sprinkle, J. R.; Riccobono, J. R.; Loach, P. A. Isolation and Characterization of a Subunit Form of the Light-Harvesting Complex of Rhodospirillum Rubrum. *Biochemistry* **1987**, *26*, 5055-5062.
(18) Visschers, R. W.; Chang, M. C.; van Mourik, F.; Parkes-Loach, P. S.; Heller, B. A.; Loach, P. A.; van Grondelle, R. Fluorescence Polarization and Low-Temperature Absorption Spectroscopy of a Subunit Form of Light-Harvesting Complex I from Purple Photosynthetic Bacteria. *Biochemistry* **1991**, *30*, 5734-5742.
(19) Fiedor, L.; Scheer, H. Trapping of an Assembly Intermediate of Photosynthetic LH1 Antenna Beyond B820 Subunit. *J.Biol.Chem.* **2005**, *280*, 20921-20926.
(20) Nakagawa, K.; Suzuki, S.; Fujii, R.; Gardiner, A. T.; Cogdell, R. J.; Nango, M.; Hashimoto, H. Probing the Effect of the Binding Site on the Electrostatic Behavior of a Series of Carotenoids Reconstituted into the Light-Harvesting 1 Complex from Purple Photosynthetic Bacterium *Rhodospirillum Rubrum* Detected by Stark Spectroscopy. *J.Phys.Chem.B* **2008**, *112*, 9467-9475.
(21) Karrasch, S.; Bullough, P. A.; Ghosh, R. 8.5a Projection Map of the Light-Harvesting Complex I from *Rhodospirillum Rubrum* Reveals a Ring Composed of 16 Subunits. *EMBO J.* **1995**, *14*, 631-638.
(22) Walz, T.; Ghosh, R. Two-Dimensional Crystallization of the Light-Harvesting I Reaction Centre Photounit from Rhodospirillum Rubrum. *J.Mol.Biol.* **1997**, *265*, 107-111.
(23) Scherz, A.; Parson, W. W. Exciton Interactions in Dimers of Bacteriochlorophyll and Related Molecules. *Biochim.Biophys.Acta* **1984**, *766*, 666-678.
(24) Alden, R. G.; Johnson, E.; Nagarajan, V.; Parson, W. W.; Law, C. J.; Cogdell, R. J. Calculations of Spectroscopic Properties of the LH2 Bacteriochlorophyll-Protein Antenna Complex from Rhodopseudomonas Acidophila. *J.Phys.Chem.B* **1997**, *101*, 4667-4680.
(25) Beekman, L. M. P.; Steffen, M.; van Stokkum, I. H. M.; Olsen, J. D.; Hunter, C. N.; Boxer, S. G.; van Grondelle, R. Characterization of the Light-Harvesting Antennas of Photosynthetic Purple Bacteria by Stark Spectroscopy. 1. LH1 Antenna Complex and the B820 Subunit from *Rhodospirillum Rubrum*. *J.Phys.Chem.B* **1997**, *101*, 7284-7292.

(26) Monshouwer, R.; Abrahamsson, M.; van Mourik, F.; van Grondelle, R. Superradiance and Exciton Delocalization in Bacterial Photosynthetic Light-Harvesting Systems. *J.Phys.Chem.B* **1997**, *101*, 7241-7248.
(27) Hu, X.; Ritz, T.; Damjanovic, A.; Schulten, K. Pigment Organization and Transfer of Electronic Excitation in the Photosynthetic Unit of Purple Bacteria. *J.Phys.Chem.B* **1997**, *101*, 3854-3871.
(28) Sundström, V.; Pullerits, T.; van Grondelle, R. Photosynthetic Light-Harvesting: Reconciling Dynamics and Structure of Purple Bacterial LH2 Reveals Function of Photosynthetic Unit. *J.Phys.Chem.B* **1999**, *103*, 2327-2346.
(29) van Grondelle, R.; Novoderezhkin, V. Dynamics of Excitation Energy Transfer in the LH1 and LH2 Light-Harvesting Complexes of Photosynthetic Bacteria. *Biochemistry* **2001**, *40*, 15057-15068.
(30) Renger, T.; May, V.; Kühn, O. Ultrafast Excitation Energy Transfer Dynamics in Photosynthetic Pigment-Protein Complexes. *Phys.Reports Rev.Sect.Phys.Lett.* **2001**, *343*, 137-254.
(31) van Grondelle, R.; Novoderezhkin, V. I. Energy Transfer in Photosynthesis: Experimental Insights and Quantitative Models. *Phys.Chem.Chem.Phys.* **2006**, *8*, 793-807.
(32) Freiberg, A.; Timpmann, K.; Jackson, J. A.; Lin, S.; Woodbury, N. W. Exciton Relaxation and Transfer in the Antenna Network of Photosynthetic Bacteria. In *Photosynthesis: Mechanism and Effects / Xi. Int. Congr. Photosynthesis Budapest 1998*; Garab, G., Ed.; Kluwer Academic Publishers: Dordrecht, 1998; pp 771.
(33) Cheng, Y. C.; Fleming, G. R. Dynamics of Light Harvesting in Photosynthesis. *Annu.Rev.Phys.Chem.* **2009**, *60*, 241-262.
(34) Scholes, G. D.; Fleming, G. R.; Olaya-Castro, A.; van Grondelle, R. Lessons from Nature About Solar Light Harvesting. *Nat.Chem.* **2011**, *23*, 763-774.
(35) Novoderezhkin, V.; Monshouwer, R.; van Grondelle, R. Disordered Exciton Model for the Core Light-Harvesting Antenna of Rhodopseudomonas Viridis. *Biophys.J.* **1999**, *77*, 666-681.
(36) Jimenez, R.; van Mourik, F.; Yu, J. Y.; Fleming, G. R. Three-Pulse Photon Echo Measurements on LH1 and LH2 Complexes of Rhodobacter Sphaeroides: A Nonlinear Spectroscopic Probe of Energy Transfer. *J.Phys.Chem.B* **1997**, *101*, 7350-7359.
(37) Chachisvilis, M.; Kühn, O.; Pullerits, T.; Sundström, V. Excitons in Photosynthetic Purple Bacteria: Wavelike Motion or Incoherent Hopping? *J.Phys.Chem.B* **1997**, *101*, 7275-7283.
(38) Novoderezhkin, V.; Monshouwer, R.; van Grondelle, R. Exciton (De)Localization in the LH2 Antenna of *Rhodobacter Sphaeroides* as Revealed by Relative Difference Absorption Measurements of the LH2 Antenna and the B820 Subunit. *J.Phys.Chem.B* **1999**, *103*, 10540-10548.
(39) Pullerits, T.; Chachisvilis, M.; Sundström, V. Exciton Delocalization Length in the B850 Antenna of *Rhodobacter Sphaeroides*. *J.Phys.Chem.* **1996**, *100*, 10787-10792.
(40) Damjanovic, A.; Kosztin, I.; Kleinekathöfer, U.; Schulten, K. Excitons in a Photosynthetic Light-Harvesting System: A Combined Molecular Dynamics, Quantum Chemistry, and Polaron Model Study. *Phys.Rev.E* **2002**, *65*, 031919-031911-031919-031924.
(41) Leupold, D.; Stiel, H.; Teuchner, K.; Nowak, F.; Sandner, W.; Ücker, B.; Scheer, H. Size Enhancement of Transition Dipoles to One-and Two-Exciton Bands in a Photosynthetic Antenna. *Phys.Rev.Lett.* **1996**, *77*, 4675-4678.
(42) Ritz, T.; Damjanovic, A.; Schulten, K.; Zhang, J.-P.; Koyama, Y. Efficient Light Harvesting through Carotenoids. *Photosynth.Res.* **2000**, *66*, 125-144.
(43) Koyama, Y.; Kakitani, Y. Mechanisms of Carotenoid-to-Bacteriochlorophyll Energy Transfer in the Light Harvesting Antenna Complexes 1 and 2: Dependence on the

Conjugation Length of Carotenoids. In *Chlorophylls and Bacteriochlorophylls: Biochemistry, Biophysics, Functions and Applications*; Grimm, B., Porra, R. J., Rüdiger, W., Scheer, H., Eds.; Springer: Dordrecht, 2006; pp 431-443.

(44) Krueger, B. P.; Scholes, G. D.; Jimenez, R.; Fleming, G. R. Electronic Excitation Transfer from Carotenoid to Bacteriochlorophyll in the Purple Bacterium Rhodopseudomonas Acidophila. *J.Phys.Chem.B* **1998**, *102*, 2284-2292.

(45) Akahane, J.; Rondonuwu, F. S.; Fiedor, L.; Watanabe, Y.; Koyama, Y. Dependence of Singlet-Energy Transfer on the Conjugation Length of Carotenoids Reconstituted into the LH1 Complex from Rhodospirillum Rubrum G9. *Chem.Phys.Lett.* **2004**, *393*, 184-191.

(46) Scholes, G. D.; Harcourt, R. D.; Fleming, G. R. Electronic Interactions in Photosynthetic Light-Harvesting Complexes: The Role of Carotenoids. *J.Phys.Chem.B* **1997**, *101*, 7302-7312.

(47) Zhang, J.-P.; Fujii, R.; Qian, P.; Inaba, T.; Mizoguchi, T.; Koyama, Y.; Onaka, K.; Watanabe, Y. Mechanism of the Carotenoid-to-Bacteriochlorophyll Energy Transfer Via the S_1 State in LH2 Complexes from Purple Bacteria. *J.Phys.Chem.B* **2000**, *104*, 3683-3691.

(48) Krueger, B. P.; Scholes, G. D.; Fleming, G. R. Calculation of Couplings and Energy-Transfer Pathways between the Pigments of LH2 by the Ab Inito Transition Density Cube Method. *J.Phys.Chem.B* **1998**, *102*, 5378-5386.

(49) Polivka, T.; Sundström, V. Dark Excited States of Carotenoids: Consensus and Controversy. *Chem.Phys.Lett.* **2009**, *477*, 1-11.

(50) Fiedor, J.; Pilch, M.; Fiedor, L. Tuning the Thermodynamics of Association of Transmembrane Helices. *J.Phys.Chem.B* **2009**, *113*, 12831-12838.

(51) Fiedor, L.; Akahane, J.; Koyama, Y. Carotenoid-Induced Cooperative Formation of Bacterial Photosynthetic LH1 Complex. *Biochemistry* **2004**, *43*, 16487-16496.

(52) Pawlowicz, N. P.; Groot, M. L.; van Stokkum, I. H. M.; Breton, J.; van Grondelle, R. Charge Separation and Energy Transfer in the Photosystem II Core Complex Studied by Femtosecond Midinfrared Spectroscopy. *Biophys.J.* **2007**, *93*, 2732-2742.

(53) van Stokkum, I. H. M.; Larsen, D. S.; van Grondelle, R. Global and Target Analysis of Time-Resolved Spectra. *Biochim.Biophys.Acta* **2004**, *1657*, 82-104.

(54) Snellenburg, J.; Laptenok, S.; Seger, R.; Mullen, K. M.; van Stokkum, I. H. M. Glotaran: A Java-Based Graphical User Interface for the R Package Timp. *J.Stat.Softw.* **2012**, *49*, 1-22.

(55) Fiedor, L. Hexacoordination of Bacteriochlorophyll in Photosynthetic Antenna LH1. *Biochemistry* **2006**, *45*, 1910-1918.

(56) Visser, H. M.; Somsen, O. J. G.; van Mourik, F.; Lin, S.; van Stokkum, I. H. M.; van Grondelle, R. Direct Observation of Sub-Picosecond Equilibration of Excitation Energy in the Light-Harvesting Antenna of Rhodospirillum Rubrum. *Biophys.J.* **1995**, *69*, 1083-1099.

(57) Monshouwer, R.; Baltuska, A.; van Mourik, F.; van Grondelle, R. Time-Resolved Absorption Difference Spectroscopy of the Lh-1 Antenna of Rhodopseudomonas Viridis. *J.Phys.Chem.A* **1998**, *102*, 4360-4371.

(58) Hunter, C. N.; Bergstroem, H.; Van Grondelle, R.; Sundstroem, V. Energy-Transfer Dynamics in Three Light-Harvesting Mutants of Rhodobacter Sphaeroides: A Picosecond Spectroscopy Study. *Biochemistry* **1990**, *29*, 3203-3207.

(59) Jirsakova, V.; Reiss-Husson, F.; Ranck, J.-L.; Moya, I. Fluorescence Life-Times and Aggregation States of the Core Light Harvesting Complex B875 from Rubrivivax Gelatinosus. *Photosynth.Res.* **1997**, *54*, 35-43.

(60) Chang, M. C.; Callahan, P. M.; Parkes-Loach, P. S.; Cotton, T. M.; Loach, P. A. Spectroscopic Characterization of the Light-Harvesting Complex of Rhodospirillum Rubrum and Its Structural Subunit. *Biochemistry* **1990**, *29*, 421-429.

(61) Loach, P. A.; Parkes-Loach, P. S. Structure-Function Relationships in Core Light-Harvesting Complexes (Lhi) as Determined by Characterization of the Structural Subunit and by Reconstitution Experiments. In *Anoxygenic Photosynthetic Bacteria*; Blankenship, R. E., Madigan, M. T., Bauer, C. E., Eds.; Kluwer Academic Publishers: Dordrecht, 1995; pp 437-471.

(62) Arluison, V.; Seguin, J.; Robert, B. Biochemical Characterization of the Dissociated Forms from the Core Antenna Proteins from Purple Bacteria. *Biochemistry* **2002**, *41*, 11812-11819.

(63) Picorel, R.; Belanger, G.; Gingras, G. Antenna Holochrome B880 of Rhodospirillum Rubrum S1. Pigment, Phospholipid, and Polypeptide Composition. *Biochemistry* **1983**, *22*, 2491-2497.

(64) Valkunas, L.; Trinkunas, G.; Liuolia, V.; van Grondelle, R. Nonlinear Annihilation of Excitations in Photosynthestic Systems. *Biophys.J.* **1995**, *69*, 1117-1129.

(65) Theiss, C.; Leupold, D.; Moskalenko, A. A.; Razjivin, A. P.; Eichler, H. J.; Lokstein, H. Femtosecond Spectroscopy of Native and Carotenoidless Purple-Bacterial LH2 Clarifies Functions of Carotenoids. *Biophys.J.* **2008**, *94*, 4808-4811.

(66) Lambrev, P. H.; Schmitt, F. J.; Kussin, S.; Schoengen, M.; Várkonyi, Z.; Eichler, H. J.; Garab, G.; Renger, G. Functional Domain Size in Aggregates of Light-Harvesting Complex Ii and Thylakoid Membranes. *Biochim.Biophys Acta* **2011**, *1807*, 1022-1031.

(67) Polivka, T.; Pullerits, T.; Herek, J. L.; Sundström, V. Exciton Relaxation and Polaron Formation in LH2 at Low Temperature. *J.Phys.Chem.B* **2000**, *104*, 1088-1096.

(68) Novoderezhkin, V. I.; van Grondelle, R. Exciton-Vibrational Relaxation and Transient Absorption Dynamics in LH1 of Rhodopseudomonas Viridis: A Redfield Theory Approch. *J.Phys.Chem.B* **2002**, *106*, 6025-6037.

(69) Gradinaru, C. C.; Kennis, J. T. M.; Papagiannakis, E.; van Stokkum, I. H. M.; Cogdell, R. J.; Fleming, G. R.; Niederman, R. A.; van Grondelle, R. An Unusual Pathway of Excitation Energy Deactivation in Carotenoids: Singlet-to-Triplet Conversion on an Ultrafast Timescale in a Photosynthetic Antenna. *Proc.Natl.Acad.Sci.USA* **2001**, *98*, 2364-2369.

(70) Papagiannakis, E.; Das, S. K.; Gall, A.; van Stokkum, I. H. M.; Robert, B.; van Grondelle, R.; Frank, H. A.; Kennis, J. T. M. Light Harvesting by Carotenoids Incorporated into the B850 Light-Harvesting Complex from *Rhodobacter Sphaeroides* R-26.1: Excited-State Relaxation, Ultrafast Triplet Formation, and Energy Transfer to Bacteriochlorophyll. *J.Phys.Chem.B* **2003**, *107*, 5642-5649.

(71) Papagiannakis, E.; Kennis, J. T. M.; van Stokkum, I. H. M.; Cogdell, R. J.; van Grondelle, R. An Alternative Carotenoid-to-Bacteriochlorophyll Energy Transfer Pathway in Photosynthetic Light Harvesting. *Proc.Natl.Acad.Sci.USA* **2002**, *99*, 6017-6022.

(72) Novoderezhkin, V. I.; Cohen, S. T. A.; van Grondelle, R. Dynamics of Exciton Relaxation in LH2 Antenna Probed by Multipulse Nonlinear Spectroscopy. *J.Phys.Chem.A* **2011**, *115*, 3834-3844.

(73) Abramavicius, D.; Valkunas, L.; van Grondelle, R. Exciton Dynamics in Ring-Like Photosynthetic Light-Harvesting Complexes: A Hopping Model. *Phys.Chem.Chem.Phys.* **2004**, *6*, 3097-3105.

(74) Bradforth, S. E.; Jimenez, R.; van Mourik, F.; van Grondelle, R.; Fleming, G. R. Excitation Transfer in the Core Light-Harvesting Complex (LH-1) of Rhodobacter Sphaeroides: An Ultrafast Fluorescence Depolarization and Annihilation Study. *J.Phys.Chem.* **1995**, *99*, 16179-16191.

Table 1. Fractions of quenched lifetimes in Ni-LH1 at different excitation wavelengths

λ_{pump} **(nm)**	Q_y (1.9 ps)	A1 (12 ps)	A2 (108 ps)
509	47%	28%	25%
590	42%	27%	31%
860	55%	21%	24%

FIGURE CAPTIONS

Figure 1. Absorption spectra of reconstituted LH1 complexes from *Rhodospirillum rubrum*. A. Carotenoid-less control LH1 and Ni-BChl-containing Ni-LH1 complexes. B. Control Sph-LH1 and Sph-Ni-LH1 (reconstituted with spheroidene).

Figure 2. Representative AFM images of Crt-less LH1. A – control sample, silicon cantilever (NSG01 NT-MDT) with force constant of 5.5 N/m, curvature radius of 10 nm and resonant frequency of 120-190 kHz. B – Ni-BChl-containing sample, MiroMasch Hi'RES-W14 cantilever, force constant 5.7 N/m, radius 1 nm, resonant frequency 160 kHz. Scale bar – 100 nm, color scale range – 4.5 nm. Lowering of the concentration of β-OG promotes oligomerization of the peptide subunits into oligomeric ring-like antenna complexes and at the same time aggregation of the complexes.

Figure 3. Absorption difference time traces of LH1 reconstituted without Ni-BChl (A) and with Ni-BChl (B) and without or with spheroidene (black and orange lines respectively). Absorption changes were probed at the wavelength of maximal bleaching after excitation at the BChl Qx band (590 nm).

Figure 4. Absorption difference time traces of control Sph-LH1 (A) and Sph-Ni-LH1 (B). Absorption changes were probed at the wavelength of maximal bleaching after excitation at the carotenoid S_2 (509 nm, green), BChl Q_x (590 nm, orange), or BChl Q_y band (860 nm, red).

Figure. 5. Evolution-associated absorption difference spectra (EADS) obtained with a sequential kinetic model fit to the pump-probe data of Crt-less LH1 (A), Sph-LH1 (B), Crt-less Ni-LH1 (C), and Sph-Ni-LH1. Excitation was at the BChl Qx band – 590 nm. The TA data were fitted with a sequential kinetic model with the initially populated state evolving by a series of irreversible steps with increasing lifetimes and the final step is relaxation to the ground state.

Figure. 6. Evolution-associated absorption difference spectra (EADS) for Sph-LH1 and Sph-Ni-LH1 data obtained with pump wavelength of 509 nm. The TA data were fitted with a sequential kinetic model with the initially populated state evolving by a series of irreversible steps with increasing lifetimes and the final step is relaxation to the ground state.

Fig. 7. Kinetic scheme of the model used for simultaneous global target analysis of the TA data obtained from Sph-Ni-LH1. The species compartments S_2, S_1, S*, and T_1 represent Sph excited states and Q_x, Q_y^0, and Q_y represent BChl excited states. The initially populated compartments were S_2, Q_x, and Q_y^0 for the 509, 590, and 860 nm pump wavelengths, respectively. Compartments A1 and A2 are populated as Q_y and represent sample heterogeneity. The fitted rate constants (ps^{-1}) are shown next to the arrows.

Fig. 8. Species-associated absorption difference spectra (SADS) resulting from global target analysis of the TA data for Sph-Ni-LH1, performed using the kinetic model shown in Fig. 7.

Figure 1

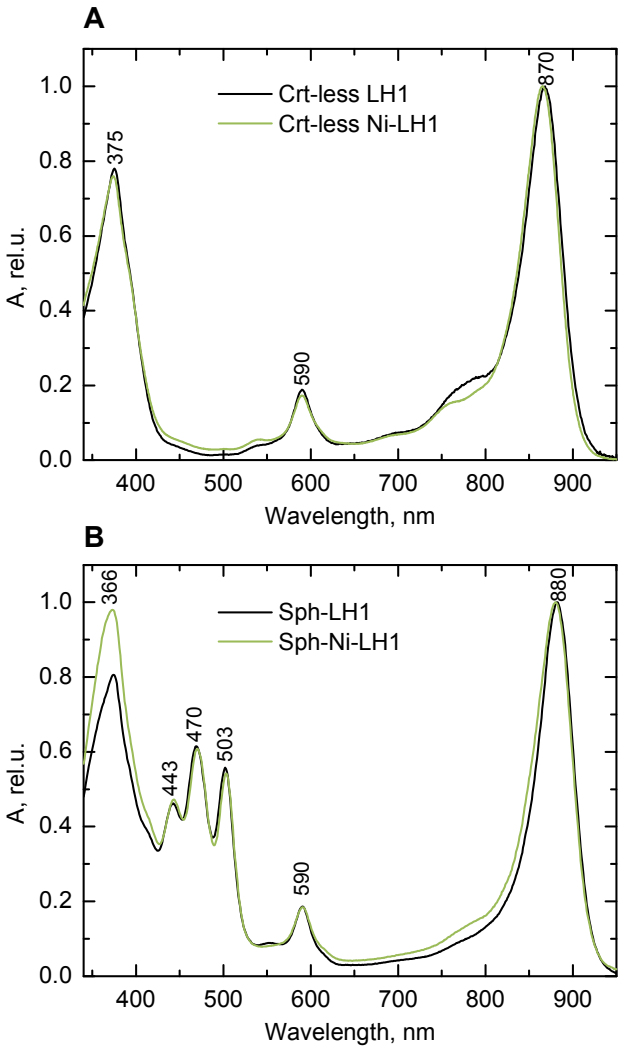
A
Crt-less LH1
Crt-less Ni-LH1
375
590
870
A, rel.u.
Wavelength, nm
B
Sph-LH1
Sph-Ni-LH1
366
443
470
503
590
880
A, rel.u.
Wavelength, nm

Figure 2

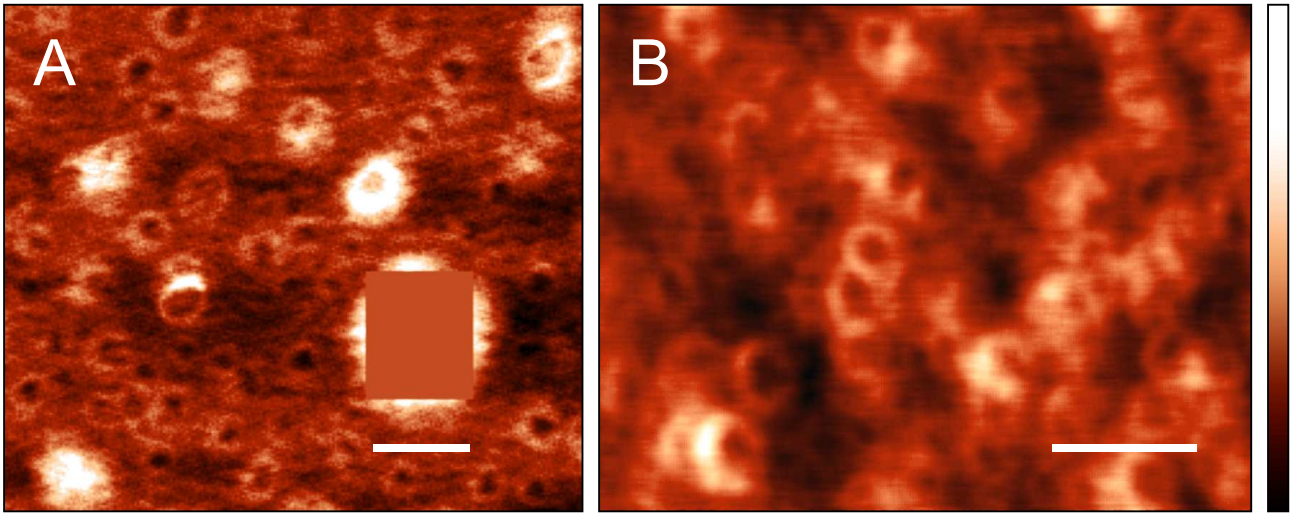

Figure 3

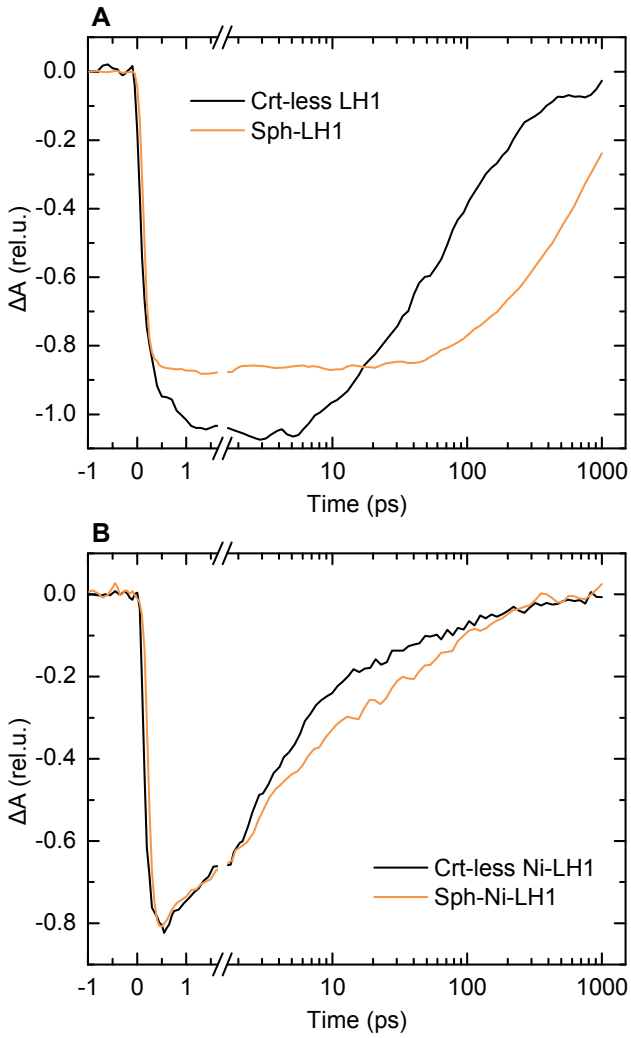
A
0.0
-0.2
-0.4
-0.6
-0.8
-1.0
ΔA (rel.u.)
Crt-less LH1
Sph-LH1
-1
0
1
10
100
1000
Time (ps)
B
0.0
-0.2
-0.4
-0.6
-0.8
ΔA (rel.u.)
Crt-less Ni-LH1
Sph-Ni-LH1
-1
0
1
10
100
1000
Time (ps)

Figure 4

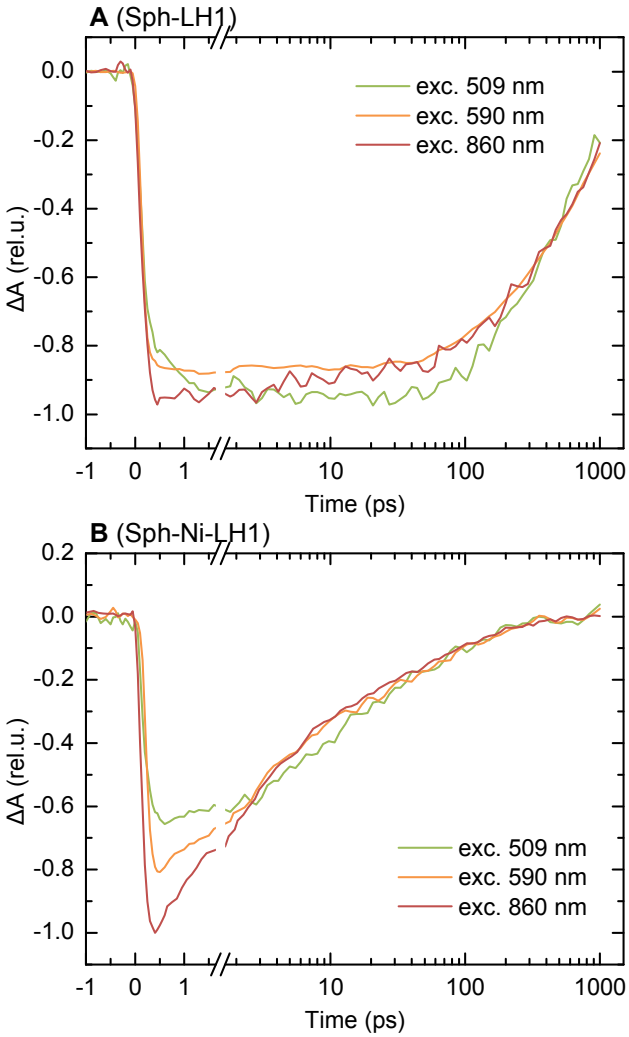
A (Sph-LH1)
0.0
-0.2
-0.4
-0.6
-0.8
-1.0
ΔA (rel.u.)
exc. 509 nm
exc. 590 nm
exc. 860 nm
-1
0
1
10
100
1000
Time (ps)
B (Sph-Ni-LH1)
0.2
0.0
-0.2
-0.4
-0.6
-0.8
-1.0
ΔA (rel.u.)
exc. 509 nm
exc. 590 nm
exc. 860 nm
-1
0
1
10
100
1000
Time (ps)

Figure 5

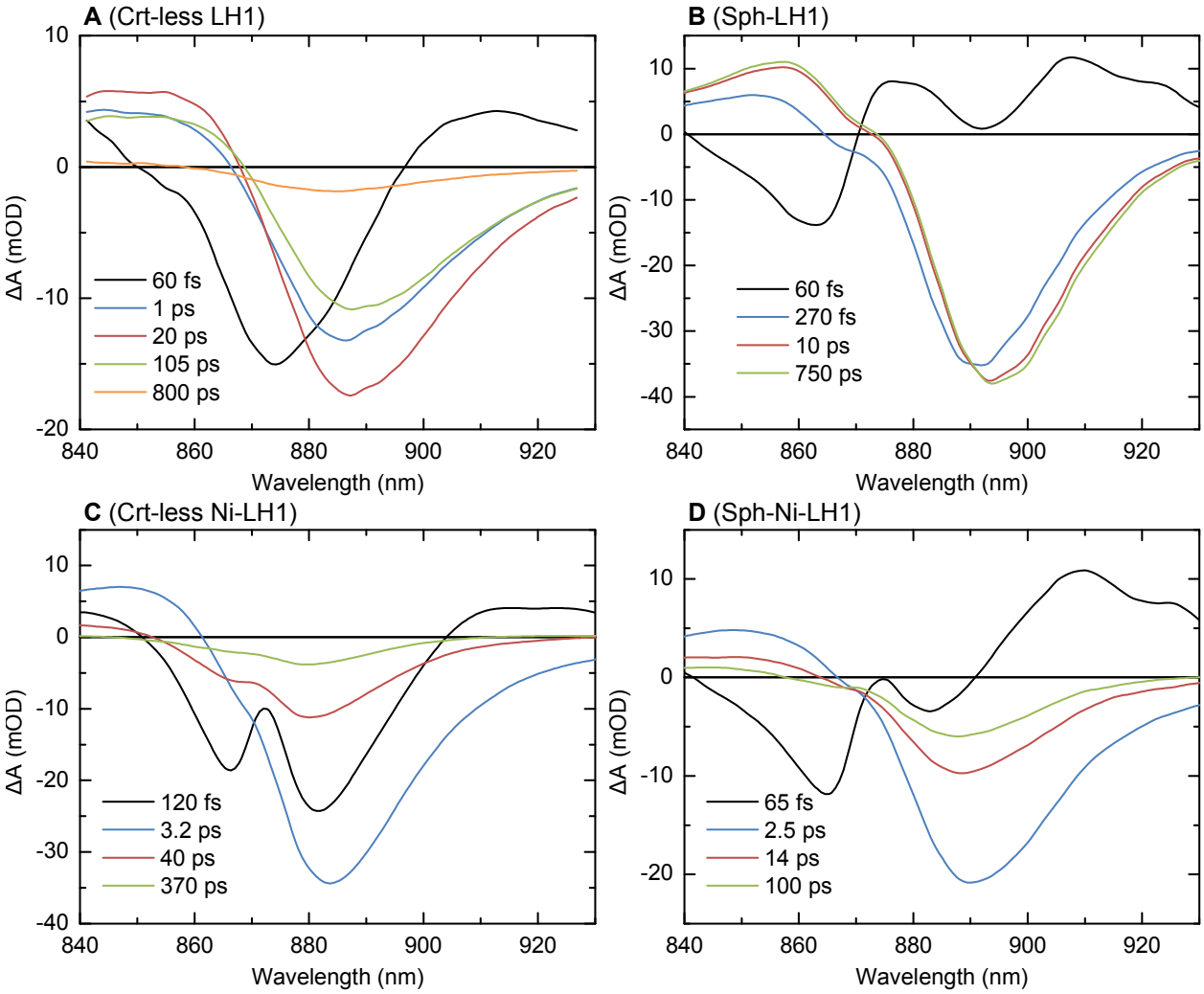
A (Crt-less LH1)
ΔA (mOD)
Wavelength (nm)
60 fs
1 ps
20 ps
105 ps
800 ps
B (Sph-LH1)
60 fs
270 fs
10 ps
750 ps
C (Crt-less Ni-LH1)
120 fs
3.2 ps
40 ps
370 ps
D (Sph-Ni-LH1)
65 fs
2.5 ps
14 ps
100 ps

Figure 6

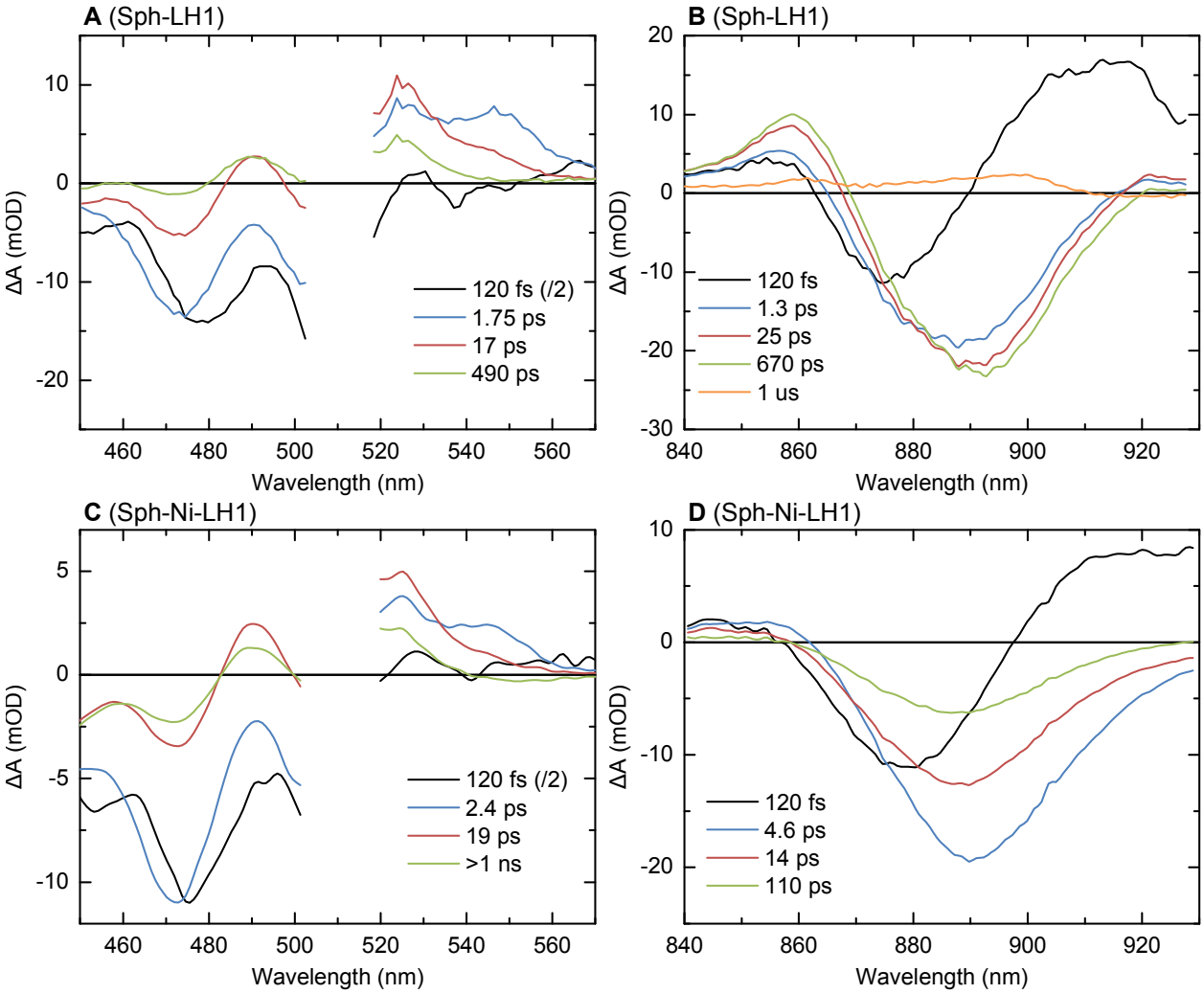
A (Sph-LH1)
ΔA (mOD)
Wavelength (nm)
120 fs (/2)
1.75 ps
17 ps
490 ps
B (Sph-LH1)
ΔA (mOD)
Wavelength (nm)
120 fs
1.3 ps
25 ps
670 ps
1 us
C (Sph-Ni-LH1)
ΔA (mOD)
Wavelength (nm)
120 fs (/2)
2.4 ps
19 ps
>1 ns
D (Sph-Ni-LH1)
ΔA (mOD)
Wavelength (nm)
120 fs
4.6 ps
14 ps
110 ps

Figure 7

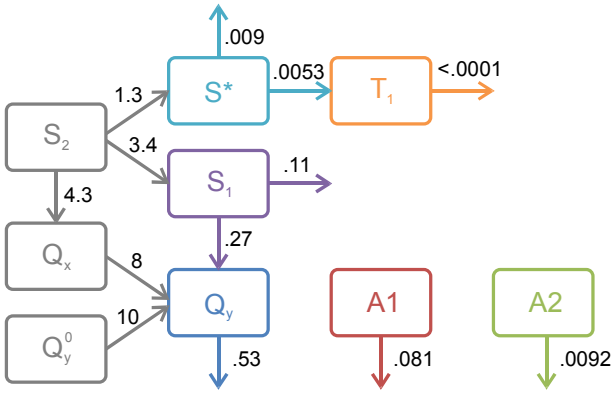
.009
S*
.0053
T1
<.0001
1.3
S2
3.4
S1
.11
4.3
.27
Qx
8
Qy
A1
A2
10
Q0y
.53
.081
.0092

Figure 8

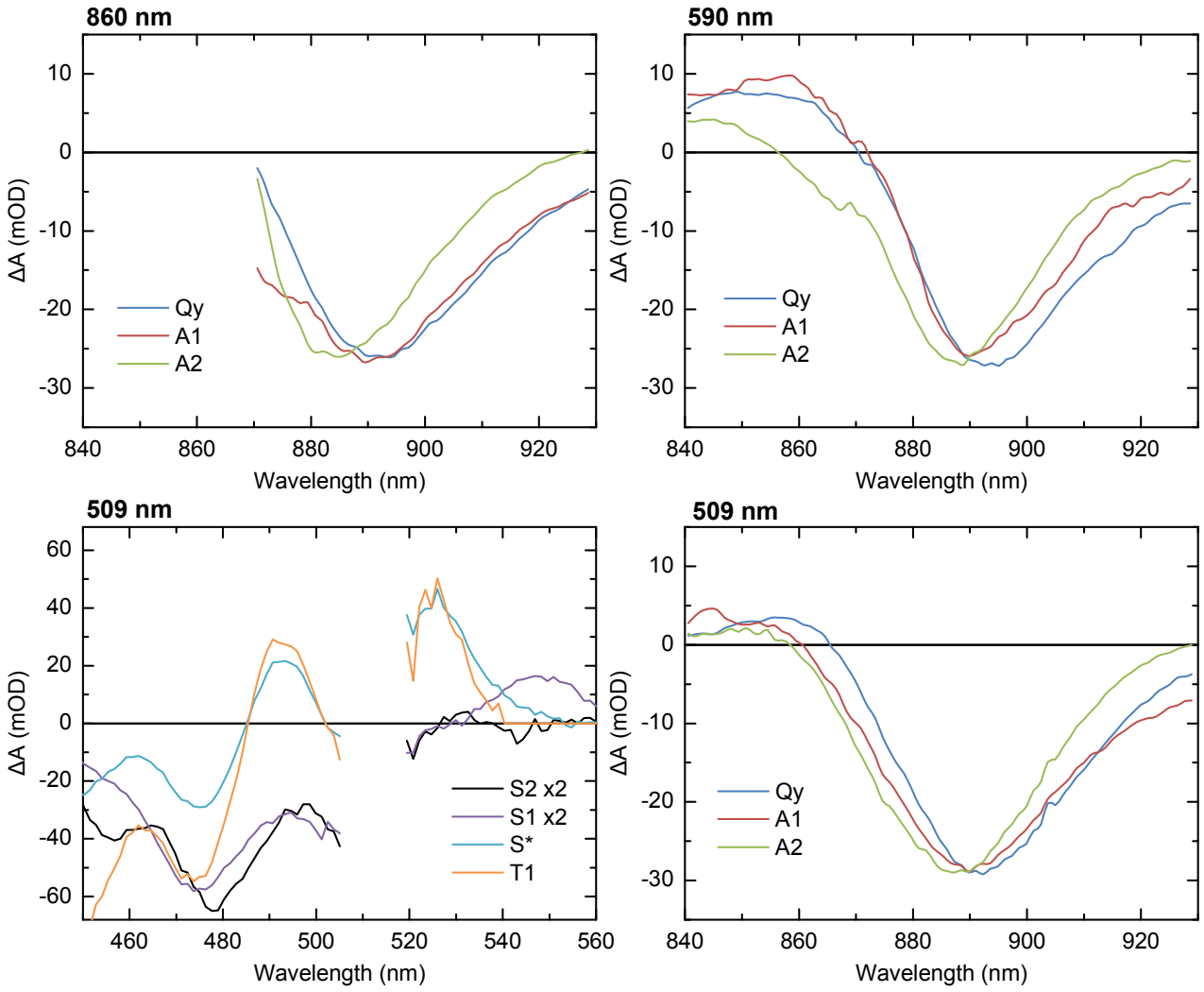
860 nm
590 nm
509 nm
509 nm
ΔA (mOD)
Wavelength (nm)
Qy
A1
A2
S2 x2
S1 x2
S*
T1

TOC graphic